THE JOURNAL OF PHYSICAL CHEMISTRY C

Article

Cite This: J. Phys. Chem. C 2019, 123, 19052−19065

pubs.acs.org/JPCC

Computational Investigation of Aqueous Phase Effects on the Dehydrogenation and Dehydroxylation of Polyols over Pt(111)

Mohammad Saleheen,[†] Mehdi Zare,[†] Muhammad Faheem,[‡] and Andreas Heyden*[,†]

[†]Department of Chemical Engineering, University of South Carolina, 301 Main Street, Columbia, South Carolina 29208, United States

[‡]Department of Chemical Engineering, University of Engineering & Technology, Lahore 54890, Pakistan

Supporting Information

ABSTRACT: Prediction of solvation effects on the kinetics of elementary reactions occurring at metal−water interfaces is of high importance for the rational design of catalysts for the biomass and electrocatalysis communities. A lack of knowledge of the reliability of various computational solvation schemes for processes on metal surfaces is currently a limiting factor. Using a multilevel quantum mechanical/molecular mechanical (QM/MM) description of the potential energy surface, we determined characteristic time and length scales for typical free-energy perturbation (FEP) calculations of bond cleavages in ethylene glycol, a sugar surrogate molecule, over Pt(111). Our approach is based on our explicit solvation model for metal surfaces and the repetition of FEP calculations to estimate confidence intervals. Results indicate that aqueous phase effects on the free energies of elementary processes can be determined with 95% confidence intervals from limited configuration space sampling and the fixed charge approximation used in the QM/MM-FEP methodology of smaller 0.1 eV. Next, we computed the initial O−H, C−H, and C−OH bond cleavages in ethylene glycol over Pt(111) in liquid water utilizing two different metal−water interaction potentials. Our calculations predict that aqueous phase effects are small (<0.1 eV) for the C−H bond cleavage and the activation barrier of the C−OH bond cleavage. In contrast, solvation effects are large (>0.35 eV) for the O−H bond cleavage and the reaction free energy of the C−OH bond scission. While the choice of a different Pt−water force field can lead to differences in predicted solvation effects of up to 0.2 eV, the differences are usually smaller (<0.1 eV), and the trends are always the same. In contrast, implicit solvation methods appear to currently not be able to reliably describe solvation effects originating from hydrogen bonding for metal surfaces even qualitatively.

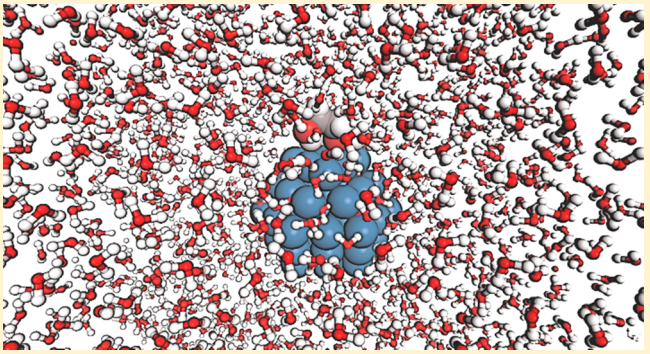

1. INTRODUCTION

The ubiquitous nature of solvents and their pervasive usage in the chemical industry[1] makes the study of solvent effects an important area of investigation. The fact that the presence and nature of solvents can affect chemical equilibria was recognized as early as 1896 with the concurrent revelation of the keto-enol tautomerism in 1,3-dicarbonyl compounds and the nitro-isonitro tautomerism of primary and secondary nitro compounds.[2−5] As evidenced by the seminal work of Menschutkin,[6] it was also demonstrated early on that the rate of chemical reactions can be attuned through the prudent choice of solvents. The role of solvents in homogeneous catalysis has long been systematically investigated and appropriated for industrial applications for several hydrogen addition and abstraction processes,[7,8] oxosynthesis,[9−12] cross-coupling reactions,[13−15] cycloadditions,[16,17] etc. One prominent example of the industrial practice of solvent effects is the aqueous two-phase catalysis in hydroformylation, which helps overcome the fundamental hurdle of homogeneously catalyzed processes, namely, the separation of catalyst and product.[18] Solvents have also been reported to affect the activity and selectivity of certain heterogeneously catalyzed hydrogenations,[19−25] oxidations,[26−30] and electrochemical reactions.[31−34] It is now predominantly acknowledged that solvents have pronounced effects on reaction equilibria, reaction pathways, yields, and product selectivity. Therefore, it is no wonder that liquid-phase processing technologies are exceedingly sought after for the heterogeneously catalyzed conversion of highly functionalized lignocellulosic biomass, which have the potential to reduce process cost and increase the target product selectivity. To design highly active, selective, and robust catalysts for these processes, there is a critical need to gain a molecular level understanding of the chemical reactions at the solid−liquid interface. By understanding the role of the solvent for surface-catalyzed reactions, solvent properties can be chosen to tailor the catalyst activity and selectivity. This

Received: May 26, 2019
Revised: July 9, 2019
Published: July 12, 2019

DOI: 10.1021/acs.jpcc.9b04994
J. Phys. Chem. C 2019, 123, 19052−19065

process of "solvent engineering" could lead to the design of more selective and less energy intensive processes for challenging chemical transformations such as the conversion of biomass. Despite considerable progress in our understanding of the stability and the surface properties of metal-supported nanoparticles in gas-phase environments, the effect of a liquid phase is less investigated and not well understood, partly due to the limited availability of experimental (in situ and in operando)[28,35−38] and theoretical studies[25,30,39−41] and partly due to the added complexity of a reaction system containing both a complex heterogeneous catalyst and a condensed phase.

Including the effect of a liquid-phase environment to chemical reactions occurring at solid−liquid interfaces is an intricate challenge in computational chemistry due to the enormity of the tasks in hand, namely, (1) an all-atomistic quantum mechanical description of the chemically relevant part of the system involving all the atoms and their immediate neighborhood relevant to the bond breaking and forming processes, (2) computation of partition functions in condensed phase systems where the harmonic approximation[42] is no longer valid, which requires an extensive phase space sampling on a high dimensional potential energy surface, and (3) a sufficiently large computational model system that adequately describes the long ranged electrostatic interactions between solute and solvent molecules, the nonharmonic dynamic fluctuations of the complex liquid phase, and can circumvent the pitfalls of finite-size effects.[43,44] While "on the fly" electronic structure calculations in brute force ab initio molecular dynamics (AIMD) simulations[45−47] have been employed lately to present some thought-provoking results,[30,48,49,121] the massive computational cost associated with it constrains both the size of the simulation system (a few hundred atoms) and the time scale of simulation (a few picoseconds).[50−52] An alternative approach is to use continuum solvation models, where the solvent is replaced by a continuum with an appropriate dielectric constant, and the solute is placed in cavities constructed within this continuum.[53] Although continuum solvation models provide a much faster way to approximate free energies of the reaction in solution, they perform poorly for describing the anisotropic site-specific interactions between solute and solvent molecules.[54] The need for an accurate description of the potential energy surface (level of theory), statistically relevant portrayal of the phase space, and adequate model system size, all the while keeping the computational cost affordable, can be realized by employing multilevel quantum mechanical/molecular mechanical (QM/MM) methods.[55−57] In this class of methods, the active site and the immediate reaction environment are treated from the first principles, while the nonreactive part of the system and the bulk of the solvent medium are treated using a classical molecular mechanical level of theory. We have previously developed such a hybrid QM/MM model dubbed as the explicit solvation model for metal surfaces (eSMS)[58] for describing heterogeneously catalyzed reactions at solid−liquid interfaces and applied it to describe aqueous phase effects on the C−C bond cleavage of a double dehydrogenated ethylene glycol moiety on Pt(111).

At the first glance, the use of molecular dynamics (MD) simulations in hybrid QM/MM models for equilibrium phase space sampling and computation of a potential of mean force appears trivial. The solute of interest surrounded by some number of solvent molecules is equilibrated with respect to an initial configuration, and dependent on the correlation time of the solvent molecules, the phase space is sampled by collecting assorted snapshots from the MD trajectories. The so-called "equilibration" stage ensures that by the end of this stage, the system is sampling from a proper thermodynamic ensemble, that is, the averages and probability of localized fluctuations of thermodynamic properties follow statistical equilibrium rules. However, the significant computational effort needed for phase space sampling, paired with the requirement for results converged to the appropriate level of accuracy to answer the problem at hand leads to a desire to identify a priori the required timescale for the equilibration and sampling phase of the MD simulations. This knowledge is particularly relevant also if a high level of theory such as DFT is needed to describe the entire simulation system, instead of a QM/MM level of theory. Only with such knowledge can we estimate whether enough computational resources are available for a given level of theory. Next, finite size effects are ubiquitous in many simulation phenomena.[59,60] For example, ensemble size effects[61,62] that arise from a too small number of particles in a simulation system and implicit or anomalous size effects[59,63,64] that can originate from an artificial stabilization of the system due to imposing an infinite periodicity are common challenges. Thus, for practical computations of solvation effects in heterogeneous catalysis, it is essential to possess a knowledge of a characteristic system size required for converged simulation results.

In a previous study, we performed a detailed first-principles vapor and aqueous phase (implicit solvation) investigation of ethylene glycol (EG) reforming over a Pt(111) model surface.[65] Our calculations suggested the primary O−H scission and the subsequent α-H abstraction to be the key rate controlling steps over a wide range of temperatures (373−673 K). We then employed our QM/MM minimum free-energy path (QM/MM-MFEP) methodology to calculate the aqueous phase effects on the abovementioned bond cleavages (without optimization in the aqueous phase).[54] Our results indicated that the aqueous phase has a much larger effect on the free energy of reaction and the free energy of activation of O−H splitting compared to that of C−H splitting. In this study, using the O−H splitting of ethylene glycol as a case study, we first identify convergence criteria for our QM/MM calculations, namely, the required timescale for equilibration, the required amount of phase space sampling, and the number of solvent molecules to be included in the simulation to accurately represent the physical system. Next, we investigate the initial O−H, C−H, and C−OH bond dissociations in liquid water over Pt(111) using our QM/MM-FEP methodology with two different Pt−water force fields (Spohr−Heinzinger[66] and metal potential[67]) and various implicit solvation methods.[53,68−70] Although the C−OH bond cleavage was not identified by our implicit solvation study to be rate controlling, understanding of solvation effects for C−OH bond cleavages is similarly essential to C−H and O−H bond cleavages for catalytic biomass processing.

In contrast to our previous study, all reactants, products, and transition states for the abovementioned reactions are optimized in the aqueous reaction environment. The results of these calculations suggest that aqueous phase effects are small (<0.1 eV) for the C−H bond cleavage and the activation barrier of the C−OH bond cleavage while they are large (>0.35 eV) for the O−H bond cleavage and the reaction free energy of the C−OH bond scission. While the choice of a

DOI: 10.1021/acs.jpcc.9b04994
J. Phys. Chem. C 2019, 123, 19052−19065

different Pt−water force field can lead to differences in predicted solvation effects of up to 0.2 eV, the differences are usually much smaller (<0.1 eV), and the trends are always the same. In contrast, implicit solvation methods appear to currently not be able to reliably describe these solvation effects for metal surfaces even qualitatively.

2. COMPUTATIONAL DETAILS

2.1. Planewave DFT Calculations. Vapor-phase DFT calculations were carried out by employing periodic boundary conditions as implemented in the Vienna ab initio simulation package (VASP 5.4).[71,72] A frozen-core, all-electron projector augmented wave (PAW)[73] method was utilized to avoid the singularities of Kohn−Sham wavefunctions at the nuclear positions. The number of valence electrons considered for Pt, C, O, and H are 10 ($5d^9 6s^1$), 4 ($2s^2 2p^2$), 6 ($2s^2 2p^4$), and 1 ($1s^1$), respectively. The purely quantum mechanical phenomena of electron exchange and correlation effects were accounted for by using the Perdew−Burke−Ernzerhof (PBE)[74,75] functional within the semilocal generalized gradient approximation.[76] Brillouin zone integrations have been performed with a 4 × 4 × 1 Monkhorst-Pack[77] k-point grid and electronic wavefunctions at each k-point were expanded using a discrete planewave basis set with kinetic energies limited to 400 eV. By increasing the number of k-points to 5 × 5 × 1, we observe a minimal change in surface electronic energy (∼0.02 eV), which suggests a good convergence of the electronic energies with respect to the k-mesh density. Due to the partial filling of bands for the metallic Pt, a first order smearing method (Methfessel−Paxton)[78] with a 0.10 eV smearing width was employed, which allowed us to calculate the entropic contributions due to the smearing very accurately. Dipole and quadrupole corrections (along the surface normal) to the total energy have been calculated using a modified version of the Makov−Payne[79] method and Harris corrections, based on the nonself-consistent Harris−Foulkes[80,81] functional, have been applied to the stress tensor and forces. A 4 × 4 unit cell with four layers of metal atoms (bottom two layers fixed in their bulk positions) has been employed to mimic the Pt(111) model surface in the vapor phase. The interaction between the periodic images along the surface normal has been curtailed by introducing a 15 Å vacuum gap on the top of the surface. The self-consistent field (SCF) convergence criterion for the electronic degrees of freedom of the valence electrons was set to 1.0×10^{-7} eV. Transition-state structures for the elementary processes were located using a combination of climbing image nudged elastic band[82,83] and dimer[84,85] methods. Finally, the minima and the first order saddle points were validated by computing the Hessian matrix and vibrational spectra.

2.2. Nonperiodic Cluster Calculations. Cluster model DFT calculations in vacuum have been carried out using the TURBOMOLE 7.2 program package.[86−88] Two layers of Pt atoms with a hexagonal shaped geometry (51 atoms) were chosen to model the Pt(111) cluster surfaces. The convergence of the total QM/MM energy with respect to the lateral size and depth of the cluster geometry can be found elsewhere.[58] An improved version of the default TURBOMOLE basis sets (def-bases) with split valence and polarization functions (def2-SVP)[89,90] was employed to represent the adsorbate atoms. Pt atoms were represented using scalar relativistic effective core potentials (ECPs) in conjunction with split valence basis sets augmented by polarization functions.[90,91] Electron exchange and correlation effects were accounted for by employing the PBE functional.[74,75] To speed up the calculation as recommended by TURBOMOLE, the RI-J approximation with auxiliary basis sets was used to approximate the Coulomb integrals.[92,93] An SCF convergence criterion of 1.0×10^{-7} hartree was established, and a Gauss−Chebyshev-type spherical grid, m4, was employed to perform the numerical integrations.[87]

2.3. Molecular Dynamics (MD) Simulations. MD simulations were carried out using the DL_POLY 4.03 molecular simulation program package.[94] The initial 4 × 4 Pt(111) unit cell was augmented laterally to a 16 × 20 surface with further vacuum added in the Z direction resulting in a 45.0 Å × 48.7 Å × 49.0 Å simulation box comprising of 1280 Pt atoms. The simulation box height was selected based on the work from Behler and Natarajan[95] who found that simulations of metal−water interfaces should contain a water layer of ∼40 Å height. An experimental saturated liquid water density of ∼0.8 g/cm^3 at 500 K was achieved by packing the simulation box with 2200 water molecules. Our procedure for obtaining approximately the correct water density consisted of (1) using a steam table to determine the number density of water molecules at the corresponding temperature, (2) performing an MD simulation with some reasonable water density and computing the average water density in the middle 10 Å of the simulation box, and (3) adjusting the number of water molecules in the simulation system to ensure approximately a liquid water environment in the middle of the simulation box. All metal and adsorbate atoms were kept fixed while the geometry of water molecules was constricted to that of TIP3P[96] geometry with the RATTLE algorithm,[97] a velocity version of the SHAKE algorithm,[98] in conjunction with the velocity Verlet (VV) integrator[99] to solve Newton's equations of motion. While different water models have been demonstrated to be applicable in different contexts,[100−102] the TIP3P water model has been reported to perform reasonably well for prediction of solvation energies of small molecules with diverse functional groups[103] as well as for large amino acid side-chain analogues,[100,101] and at least for small molecules, the solvation energies are reported to be not sensitive to the water model.[103] Hence, the TIP3P model was employed for the force-field parameters of liquid water while the van der Waals parameters for adsorbate atoms were obtained from the OPLS force field.[106,107] In addition to the OPLS parameters, the Lennard-Jones parameters from the CHARMM all-atom force field[102] were used for the hydrogen atoms of the adsorbed moieties. Lennard-Jones parameters for hydrogen atoms are important in QM/MM optimizations that permit hydrogen atoms to approach water molecules and leave the protective environment of a neighboring carbon or oxygen atom. Both the Spohr−Heinzinger (SH)[66] and metal potential[67] were employed to describe the Pt−water interaction. However, only the SH potential was utilized for the optimization of the adsorbed species in liquid water, because this potential has recently been found to give a better description of the water−Pt(111) interaction compared to that of the metal potential.[103] The charges for the QM atoms were estimated using the natural population analysis (NPA).[104,110] To describe the interaction of the TIP3P water point charges with the quantum chemically described cluster model, we employed the periodic electrostatic embedded cluster method (PEECM)[105] as implemented in TURBOMOLE. Simulations were carried out in a canonical ensemble (NVT) with Nosé−

DOI: 10.1021/acs.jpcc.9b04994
J. Phys. Chem. C 2019, 123, 19052−19065

Hoover thermostat.[106,107] A 1 ps relaxation time constant for temperature fluctuations was used to maintain the average system temperature. Electrostatic interactions were accounted for by using the smoothed particle mesh Ewald (SPME) method[108,114] with automatic parameter optimization for default SPME precision, and a 12 Å cutoff radius was adopted for the van der Waals interactions and the transition between short- and long-range electrostatic interactions. If not specified differently, all systems were equilibrated for 250 ps and sampled for 725 ps using a 1 fs timestep. To optimize structures in an aqueous reaction environment, we utilized the fixed size ensemble approximation with 10,000 MM conformations recorded every 50 fs. Although we are modeling metal−water interfaces, our time interval for recording structures is based on a recent study of liquid water by Cowan et al.[109] who concluded that "liquid water essentially loses the memory of persistent correlations in its structure within 50 fs".

2.4. QM/MM Energy Calculation. A QM/MM minimum free-energy path (QM/MM-MFEP)[56,57] method for optimizing the intrinsic reaction coordinate on a potential of mean force (PMF) description of the reaction system has been implemented in our program packages. A full description of this methodology, explicit solvation for metal surfaces (eSMS), can be found elsewhere.[58] It should be noted here that each QM/MM energy evaluation requires one single-point periodic DFT calculation using VASP, one periodic electrostatic embedding calculation using TURBOMOLE, one nonperiodic DFT calculation of the cluster model using TURBOMOLE, single-point MD calculations on 100 reference structures (100 equidistant conformations along the trajectory generated in the absence of any QM charges), and an ensemble of single-point MD calculations on conformations along the trajectory generated (with ESP fitted charges on the QM atoms). Free-energy calculations require energy evaluation from uncorrelated measurements of the system, and ideally, the energy estimator should also be capable of minimizing the statistical bias and variance of the free-energy differences of the physical system being studied.[117] Exponential averaging (EXP), also known as the Zwanzig relationship,[116] has long been applied to study a variety of problems such as amino acid recognition,[111] RAS−RAF binding affinity,[118] and octanol/water partition coefficients,[119] etc.[112,113] However, the EXP has been shown to represent poor efficiency and phase space overlap[114,115] and also is largely dependent on the distribution of the QM/MM energy.[122] Here, we employed the Bennett acceptance ratio (BAR)[117] as the free-energy estimator that uses both the forward and reverse distributions simultaneously in a more efficient way than simply averaging the forward and reverse exponential estimators. BAR has been demonstrated to be advantageous in practical atomistic simulations as it displays a lower bias and variance of the free-energy estimates when compared to EXP and thermodynamic integration (TI).[114,118] Finally, the whole free-energy estimation procedure has been repeated three times to establish 95% confidence intervals for evaluating the free energy of reaction and free energy of activation, assuming a normal distribution.[125] All uncertainties reported in this study are 95% confidence intervals.

2.5. Periodic Implicit Solvation Calculations. In addition to implicit solvation calculations performed with the iSMS method,[41] we performed implicit solvation calculations at 500 K using VASPsol[69,70] with a relative permittivity of water of 30.55 at reaction conditions.[120] We used the default values for the parameter n_c that defines the value at which the dielectric cavity forms and for the width of the diffuse cavity.[69] We also employed the default effective surface tension parameter for describing the cavitation, dispersion, and repulsive interaction between the solute and the solvent that are not captured by the electrostatic terms.[69] While this parameter is likely most accurate only for simulations at 298 K and not at 500 K, it is an optimized parameter of the solvent model that cannot easily be obtained at other temperatures. Due to the absence of adequate experimental solvation data at 500 K, we decided that the default parameter is likely most meaningful. All other computational details for periodic implicit solvation calculations were kept the same as in our periodic vapor-phase calculations.

3. RESULTS AND DISCUSSION

The bidentate binding mode of ethylene glycol on the Pt(111) surface in vapor phase (adsorption through hydroxyl groups and formation of intramolecular hydrogen bonds due to the directionality of the hydroxyl groups, Figure S1a) makes the direct C−C and C−O bond cleavages energetically unfavorable with high activation barriers of 2.07 and 2.09 eV, respectively. In the vapor phase, the initial hydrogen abstraction from the hydroxyl group to form an alkoxide intermediate is thermodynamically unfavorable (ΔE_{rxn} = + 0.40 eV) compared to the dehydrogenation of ethylene glycol to form 1,2-dihydroxyethyl (ΔE_{rxn} = − 0.48 eV). However, due to the close proximity of the H atom of the hydroxyl group to the surface and the required rotation of the second hydroxyl group away from the surface for the C−H scission, the O−H bond cleavage is slightly more energetically favorable.[54,65] The choice of the O−H bond scission reaction to establish the characteristic parameters for a well-converged QM/MM calculation has been motivated by the fact that the activation barrier is neither too high to make the FEP procedure computationally prohibitive nor too low to make the PMF procedure ill-founded and the characterization of the aqueous phase effect extremely problematic. We have recently demonstrated that in an aqueous reaction environment, the entropy−enthalpy compensation plays a major role in facilitating the O−H bond scission on hydrophobic interfaces and exhibits a substantial solvent effect on the free energy of reaction and free energy of activation, which makes this model reaction all the more compelling for determining characteristic parameters for explicit solvation calcualtions.[54]

3.1. Timescale for Equilibration. Conventional approaches for achieving a thermal equilibrium in an MD simulation involve an equilibration stage. Although the timescale for the equilibration period is dependent on the initial phase space point and can be determined from the relaxation time of various properties and a normal distribution of their fluctuations, in practice, it is difficult to determine the slowest time scale of the simulation system, and the equilibration time scale is often determined by computational affordability (even if it risks biasing the simulation result) and therefore, varies wildly from 300 fs in AIMD simulations[127] to 10 ps in QM/MM simulations[128] and 2 ns in combined DFT-MD[123,124] investigations that use a classical force field for the equilibration stage.

Figure S4a illustrates the total energy, and Figure S4b depicts the root-mean-square fluctuations (RMSF) of the potential energy during a 975 ps MD simulation of ethylene glycol solvated by 2200 water molecules, thermally coupling all

DOI: 10.1021/acs.jpcc.9b04994
J. Phys. Chem. C 2019, 123, 19052−19065

the atoms to a Nosé−Hoover heat bath at 500 K. While the total energy graph might suggest that an equilibrated state has been obtained after ∼4 ps, the RMSF appears to be converged only after ∼200 ps. To quantify the timescale required for equilibration to predict aqueous phase effects on a surface-catalyzed reaction with a greater certainty, we performed QM/MM free-energy perturbation calculations with three distinct equilibration periods of 50, 100, and 250 ps. For each equilibration timescale, we explored the equilibrium phase space for 150 ps (1000 MM conformations, 150 fs apart) with three independent MD simulations. We employed BAR as the free-energy estimator for each individual trajectory and computed 95% confidence intervals from the three independent observations. Figure 1 and Table S1 display the variability

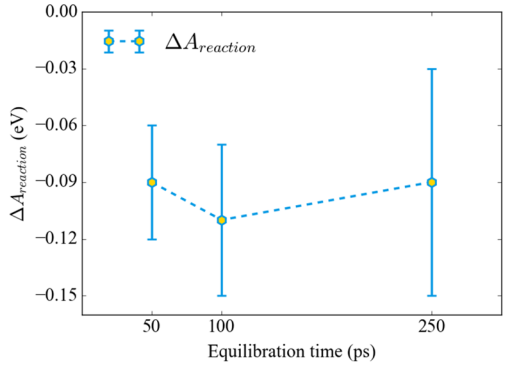

(a)

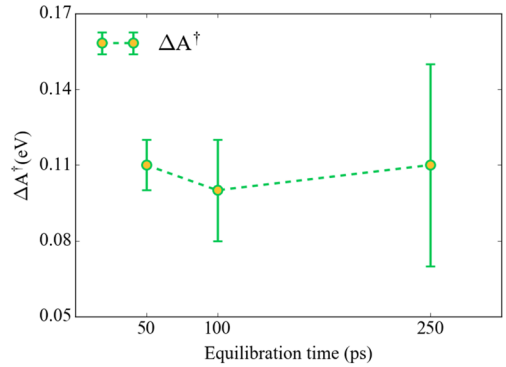

(b)

Figure 1. 95% confidence interval estimates of (a) the free energy of reaction and the (b) free energy of activation of the O−H bond cleavage of ethylene glycol over a Pt(111) surface at 500 K. Total QM/MM energies have been computed by employing three distinct equilibration times of 50, 100, and 250 ps.

in the estimation of the free energy of reaction and free energy of activation for our model reaction. Our calculations indicate that all equilibration stages lead overlapping error bars and approximately the same estimation of the free energies of reaction and activation ($\Delta A_{rxn} \approx -0.09$ eV, $\Delta A^{\dagger} \approx 0.11$ eV). Also, predicted error bars are smaller than 0.06 eV and therefore well within the inherent error of density functional theory calculations.[131] Although the error bars are slightly larger for the simulations with the longest equilibration stage, we use in the following 250 ps equilibration period for calculating aqueous phase effects on the free energies of surface-catalyzed reactions. Our selection is motivated by the high degree of the RMSF in the potential energy at and below 100 ps (Figure S4b), the fact that we do not possess estimates of the error bar of our error bars, and that we show in the next section that typical rotational water correlation times near our adsorbate are on the order of ∼40 ps.

3.2. Configuration Space Sampling. An overarching theme in the calculation of liquid-phase effects on free energies of elementary processes is the calculation of ensemble averages.[116,126] To calculate a reliable estimate of an ensemble average, the potential energy surface has to be adequately sampled for all the relevant configurations of the system. However, the sheer size of the configuration space originating from the sizable number of solvent molecules included in the simulation box makes extensive exploration of the configuration space extremely challenging. Owing to a lack of consensus on how much sampling of the configurational space is sufficient for a solvated adsorbed carbohydrate species on a metal surface for an error smaller than 0.1 eV, we computed the average rotational correlation time for water molecules in close proximity (up to 5 Å) to adsorbed ethylene glycol on Pt(111) and performed QM/MM-MFEP calculations for our test reaction with ensemble averages calculated from 100, 500, and 1000 MM conformations that are 150 fs apart (i.e., sampling for 15 to 150 ps). Figure S5 illustrates a three-exponential fit to the rotational correlation time of water molecules in close proximity to the adsorbate. The average rotational correlation lifetime is computed to be ∼40 ps. This result agrees with both the correlation time of hydrogen bonds between a water layer and a hydrocarbon species adsorbed on Pt(111) and the hydrogen bond correlation time of a water layer on various Cu surfaces, all of which have been determined to be between 1 and 10 ps.[95,124] For the free-energy calculations, the procedure was repeated three times with independent MD trajectories to establish the confidence interval estimates of the free energy of reaction (Figure 2a) and the free energy of activation (Figure 2b). Independent trajectories are obtained from trajectories separated by at least 125 ps, which are significantly larger than the correlation times discussed above. As illustrated in Figure 2, the uncertainty in the calculation of free energies is statistically indistinguishable (see also Table S2). To err on the side of the caution and sample for at least three times the correlation lifetime of water molecule rotations, we employed 1000 MM conformations for all subsequent free-energy calculations (sampling of 150 ps). A repetition of the simulations and computation of confidence intervals were found essential since the fluctuations of a single potential of mean force calculation were often significant as evidenced by 95% confidence intervals of up to 0.1 eV from three measurements. The significant fluctuations of a single potential of mean force calculation originate from both the limited phase space sampling and from the use of the fixed charge approximation used in the QM/MM-FEP methodology. We note that each FEP calculation requires one to compute the ESP charges on the QM atoms as a mean field of the electrostatic potential of 100 MM conformations. By repeating the calculations for three times, we both increase our total configuration space sampling and obtain simulation results for three slightly different ESP charges on the QM atoms, overall improving the reliability of our predictions.

3.3. System-Size Effects. The infinite periodicity of a computational simulation system makes it less susceptible to

DOI: 10.1021/acs.jpcc.9b04994
J. Phys. Chem. C 2019, 123, 19052−19065

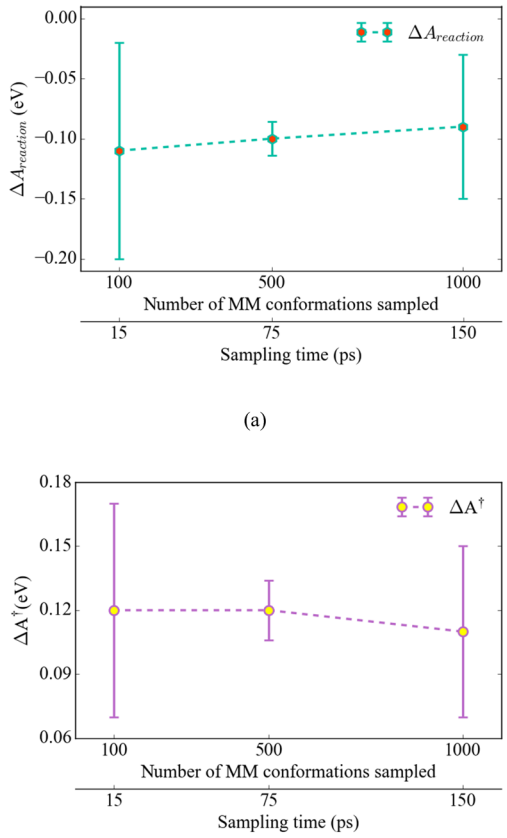

Figure 2. Effect of phase space sampling time on the estimation of (a) free energy of reaction and (b) free energy of activation of the model O−H bond scission reaction of ethylene glycol on a Pt(111) surface at 500 K. The error bars represent the 95% confidence interval estimate of the free energy of the specified reaction.

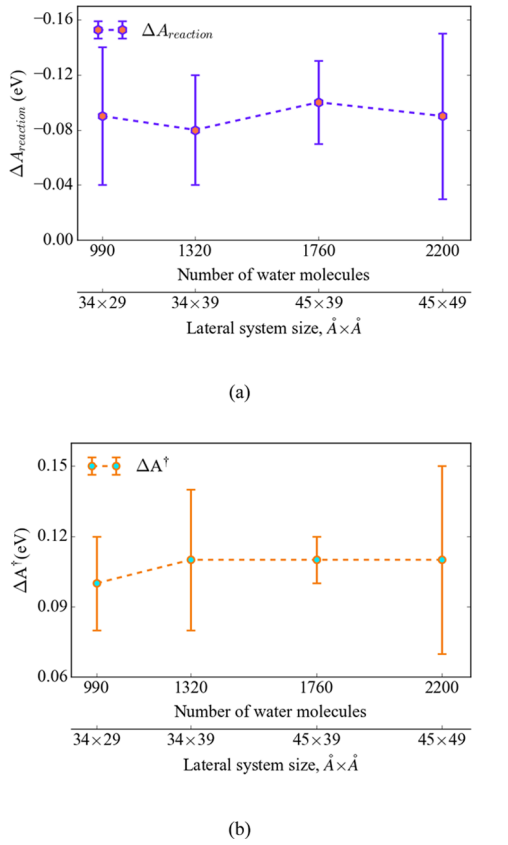

Figure 3. System-size effect on (a) free energy of reaction and (b) free energy of activation of the prototypical O−H bond cleavage reaction of ethylene glycol on a Pt(111) model surface at 500 K. The error bars represent the 95% confidence interval estimate of the free energy of the specified reaction.

finite size effects when compared to nonperiodic system simulations. However, a periodic system with a small simulation box tends to show crystal-like long-range order while an unnecessarily large simulation system might result in wasted computational resources without adding any germane information needed to describe the physical system.[133] To explore the effect of the system size on the solvent effect on free energies of our model reaction, we constructed four different simulation boxes by changing the lateral box size while maintaining a constant liquid height (49.0 Å) to keep the system pressure and density constant. In the decreasing order, the lateral dimensions of the simulation boxes are 45.0 Å × 49.0 Å, 45.0 Å × 39.0 Å, 33.7 Å × 39.0 Å, and 33.7 Å × 29.2 Å, which correspond to solvating the metal surface and adsorbate by 2200, 1760, 1320, and 990 water molecules. We note that we refrained from decreasing the box size below this point since it would result in a simulation box with the smallest dimension being less than twice the cutoff employed for calculating vdW interactions.

As shown in Figure 3, there is no statistically significant difference in the predicted free energies, and we conclude that even our smallest simulation box is likely sufficiently large for our free-energy calculations. Nevertheless, we use in the following our simulation box containing ∼2200 water molecules. While for our eSMS solvation model, the length scales of relevance are not computationally prohibitive; for a full quantum chemical description of the potential energy surface, it is interesting that correlation lengths appear to be smaller than 15 Å (half the shortest simulation box length).

3.4. Optimization of Adsorbed Moieties. Vapor-phase-optimized structures were employed as the initial configuration for the optimization of reactants, transition states, and product states of the O−H, C−OH, and C−H bond cleavages of ethylene glycol in the aqueous phase. Each optimization cycle consisted of a 750 ps MD simulation with 250 ps of the equilibration stage and 500 ps of equilibrium configuration space sampling. Geometries were then optimized in a fixed size ensemble of 10,000 MM conformations recorded at 50 fs intervals with a force-based convergence criterion of 1.0×10^{-3} au/atom. The optimized QM structure was then employed for the generation of a new ensemble of MM conformations, and the whole procedure was repeated until the QM/MM energy was converged.

Generally, the aqueous phase appears to have only a minor effect on the reactant ($\Delta A_{RS} = -0.06 \pm 0.01$ eV), product ($\Delta A_{PS} = -0.10 \pm 0.01$ eV), and transition state ($\Delta A_{TS} = 0.03 \pm 0.01$ eV) relaxations for the O−H bond cleavage.

$$CH_2OHCH_2OH^{**} + * \leftrightarrow CH_2OCH_2OH^{**} + H^* \quad (1)$$

In the reactant state, going from the vapor (Figure S1a) to an aqueous phase (Figure S1b), the Pt−O bond length increases by 0.10 Å. Similarly, the product state (Figure S1e,f) is pushed upward into the aqueous phase, and the Pt−O bond length increases by 0.78 Å. Considering the hydrophobicity of

DOI: 10.1021/acs.jpcc.9b04994
J. Phys. Chem. C 2019, 123, 19052−19065

the Pt(111) surface,[128] this places the adsorbed moiety in the immediate vicinity of the first layer of the water molecules (Figure S6), leading to many hydrogen bonding arrangements plausible with the neighboring water molecules, which results in a slightly stabilized reactant and product state. Additionally, for the reactant state, the distance between the hydrogen atom (H_2) of the nonreacting hydroxyl group and the oxygen atom of the reacting hydroxyl group (O_1) decreases by 0.18 Å, making intramolecular hydrogen bonding more probable. The transition state does not show a significant change (less than 0.02 Å) in the H_2-O_1 distance and the Pt−O bond length; only the transition-state bond length gets reduced by 0.18 Å when going from the vapor to aqueous phase.

Figures S2 and S3 illustrate the corresponding effect of an aqueous phase on the structure of various states in the C−H and C−OH bond cleavage reactions. Similar to the O−H bond cleavage, the transition state and the product state moieties of the C−OH bond cleavage reaction move upward, going from the vapor to aqueous phase, which explains their stabilization in an aqueous phase ($\Delta A_{TS} = -0.09 \pm 0.01$ eV, $\Delta A_{PS} = -0.03 \pm 0.01$ eV).

$$CH_2OHCH_2OH^{**} + * \leftrightarrow CH_2CH_2OH^{**} + OH^* \quad (2)$$

The transition-state bond length also increases by 0.10 Å due to the presence of an aqueous phase. Unlike the O−H and C−OH bond cleavages, the aqueous phase has no perceptible effect on the transition state and the product state of the C−H bond cleavage ($\Delta A_{TS} = 0.06 \pm 0.01$ eV, $\Delta A_{PS} = 0.01 \pm 0.01$ eV).

$$CH_2OHCH_2OH^{**} + * \leftrightarrow CHOHCH_2OH^{**} + H^* \quad (3)$$

Except for a minimal rotational change, both the transition state and the product state of the C−H bond cleavage largely remain unaffected by the presence of an aqueous phase, resulting in a nominal solvent effect. The transition-state bond length also remains largely unaltered (less than 0.02 Å) going from the vapor to aqueous phase.

3.5. Free-Energy Profile. Figures 4−6 illustrate the free-energy (potential of mean force) profiles for the O−H, C−H, and C−OH bond cleavages, respectively. For the O−H and C−H bond cleavages, we presented previously[54] similar profiles without the optimization of the critical points in an aqueous phase and without vdW parameters for hydrogen atoms of the adsorbate molecules that are only needed for an optimization. To establish adequate phase space overlap throughout the reaction coordinate, we introduced 41 intermediate states between the reactant and transition states and 19 intermediate states between the transition state and the product state for the O−H cleavage reaction (Figure 4). The number of windows is determined by our desire to have an energy difference between windows smaller than twice the thermal energy (<2 k_BT). Similarly, the free-energy profile for the C−H cleavage reaction (Figure 5) has been constructed by inserting 26 intermediate states between the reactant and transition states and 29 intermediate images between the transition state and the product state. Finally, the potential of mean force profile for the C−OH bond cleavage (Figure 6) has been constructed by inserting 72 intermediate states between the reactant state and the transition state and 66 intermediate images between the transition state and the product state. A summary of our calculation results is shown in Table 1 and Figure 7.

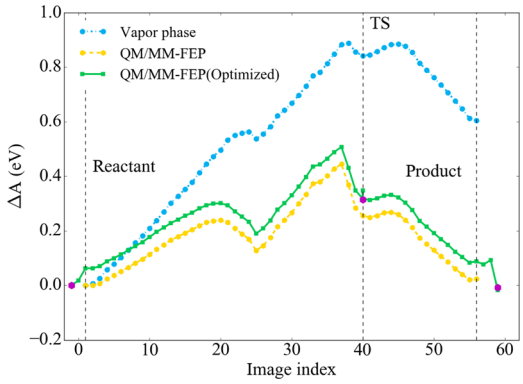

Figure 4. Free-energy profile for the O−H bond cleavage of ethylene glycol in vapor and aqueous phases on a Pt(111) model surface at 500 K without considering vibrational contributions to the partition function. See Table 1 for corresponding data that include vibrational contributions. The points lying on the vertical dashed lines represent the geometries optimized in the vapor phase, while the magenta dots on the QM/MM-FEP(Optimized) profile represent the aqueous phase-optimized structures of the reactant, transition state, and product state for the O−H bond cleavage. The aqueous phase profiles portray the average of three QM/MM-FEP calculations that possess 95% confidence intervals smaller than ±0.1 eV.

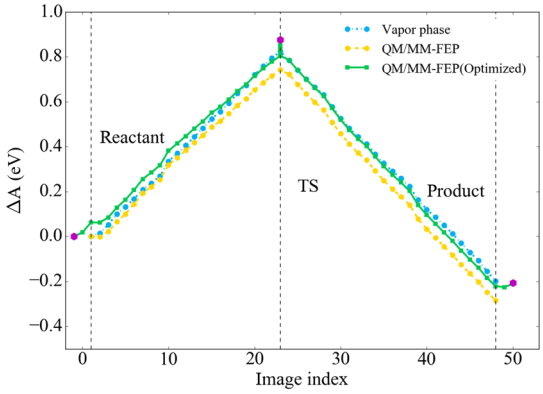

Figure 5. Free-energy profile for the C−H bond cleavage of ethylene glycol in vapor and aqueous phases on a Pt(111) model surface at 500 K without considering vibrational contributions to the partition function. See Table 1 for corresponding data that include vibrational contributions. The points lying on the vertical dashed lines represent the geometries optimized in vapor phase, while the magenta dots on the QM/MM-FEP(Optimized) profile represent the aqueous phase-optimized structures of the reactant state, transition state, and product state for the C−H bond cleavage. The aqueous phase profiles are the average of three QM/MM-FEP calculations that possess 95% confidence intervals smaller than ±0.1 eV.

Figure 7 illustrates that the aqueous phase has a much larger effect on the O−H bond scission than on the C−H and C−OH bond scissions of ethylene glycol. The free energy of the reaction of the C−OH bond scission is also significantly affected by the aqueous environment. These observations can be understood by the structural changes along the reaction coordinate in each of the abovementioned reactions. The presence of liquid water and formation of hydrogen bonds between the adsorbate and the surrounding water weakens the intramolecular hydrogen bonding (increase in distance between OH groups) for the reactant, transition state, and product state of the C−H bond cleavage. The C−H bond scission also exposes a C atom to the neighboring aqueous

DOI: 10.1021/acs.jpcc.9b04994
J. Phys. Chem. C 2019, 123, 19052−19065

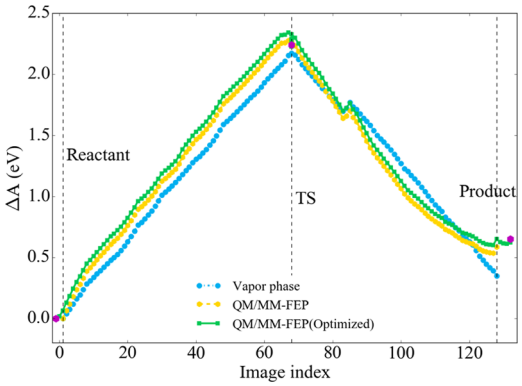

Figure 6. Free-energy profile for the C−OH bond cleavage of ethylene glycol in vapor and aqueous phases on a Pt(111) model surface at 500 K without considering vibrational contributions to the partition function. See Table 1 for corresponding data that include vibrational contributions. The points lying on the vertical dashed lines represent the geometries optimized in vapor phase, while the magenta dots on the QM/MM-FEP(Optimized) profile represent the aqueous phase-optimized structures of the reactant, transition, and product states for the C−OH bond cleavage. The aqueous phase profiles are the average of three QM/MM-FEP calculations that possess 95% confidence intervals smaller than ±0.1 eV.

phase environment, which is unable to form hydrogen bonds with the water molecules. As a result, the aqueous phase has only a very minor effect on the net hydrogen bonding along the reaction coordinate, and solvation effects are small and within the accuracy of our calculations. In contrast, the O−H bond cleavage exposes a highly electronegative O atom ($O^{\delta-}$ = − 0.74 e^-) to the surrounding environment, which is able to accept hydrogen bonds from the hydrogen atoms of the water molecules, changing the hydrogen bonding energy contribution along the reaction coordinate and resulting in a sizable exergonic solvation effect on the free energy of reaction and free energy of activation.

The presence of an aqueous phase has a significant endergonic effect on the thermodynamics of the C−OH bond cleavage while the kinetics of the reaction remains unaffected. Figure S7 shows a snapshot of the distribution of water molecules on the top of the Pt(111) surface for the reactant, transition state, and product state of C−OH bond cleavage of ethylene glycol. In the reactant state (Figure S7a), the adsorbed species (ethylene glycol) is immersed in the first layer of water molecules. However, in the product state (Figure S7c), the cleaved OH species lies beneath the layer of water molecules, which reduces the number of hydrogen bonding arrangements for the adsorbed moiety, resulting in an endergonic effect on the thermodynamics of the reaction. Unlike the O−H bond scission, the C−OH bond scission exposes a C atom to the surrounding aqueous phase environment, which is unable to form hydrogen bonds with water molecules, leading to a nominal aqueous phase effect on the kinetics of this reaction. Michel and co-workers have recently claimed that C−OH bond cleavages are promoted by the explicit presence of a water molecule (microsolvation[129−131] approach).[132] While the inclusion of water coordinates in the reaction coordinate can indeed lead to a lower activation barrier that is currently not considered in our simulations, the microsolvation approach does not sample the configuration space and therefore neglects any temperature-dependent entropic cost associated with placing a water molecule at a specific location.

3.6. Comparison of Metal−Water Interaction Potentials. The predictive power of any solvation approaches that

Table 1. Aqueous Phase Effects on the Free Energy of Reaction and the Free Energy of Activation of Model Reactions of Ethylene Glycol over Pt(111) at 500 K[a]

reaction	reaction environment	$\Delta G_{rxn}/\Delta A_{rxn}$ (eV)	$\Delta G^{\dagger}/\Delta A^{\dagger}$ (eV)
$CH_2OHCH_2OH^{**} + * \leftrightarrow CH_2OCH_2OH^{**} + H^*$	vapor phase	0.45	0.70
	iSMS	0.36	0.68
	VASPsol	0.57	0.76
	QM/MM-FEP^{SH}	−0.09 ± 0.06	0.11 ± 0.04
	QM/MM-FEP^{LJ}	0.08 ± 0.02	0.29 ± 0.01
	QM/MM-FEP^{SH}(OPT)	−0.23 ± 0.05	0.21 ± 0.03
$CH_2OHCH_2OH^{**} + * \leftrightarrow CHOHCH_2OH^{**} + H^*$	vapor phase	−0.40	0.73
	iSMS	−0.39	0.65
	VASPsol	−0.35	0.59
	QM/MM-FEP^{SH}	−0.38 ± 0.02	0.64 ± 0.02
	QM/MM-FEP^{LJ}	−0.26 ± 0.06	0.56 ± 0.01
	QM/MM-FEP^{SH}(OPT)	−0.36 ± 0.01	0.73 ± 0.02
$CH_2OHCH_2OH^{**} + * \leftrightarrow CH_2CH_2OH^{**} + OH^*$	vapor phase	0.26	2.11
	iSMS	0.15	2.04
	VASPsol	0.30	2.04
	QM/MM-FEP^{SH}	0.57 ± 0.02	2.16 ± 0.01
	QM/MM-FEP^{LJ}	0.49 ± 0.02	2.18 ± 0.01
	QM/MM-FEP^{SH}(OPT)	0.64 ± 0.03	2.11 ± 0.03

[a]QM/MM-FEP calculations describe the solvent effect on the critical points identified by gas-phase calculations while using the gas-phase vibrational partition function for the adsorbed species and transition states. The superscripts SH and LJ (SH = Spohr−Heinzinger, LJ = metal Lennard-Jones) denote the potential used to describe the metal−water interaction. QM/MM-FEP(OPT) represents the solvent effects for the model reactions (using SH potential) where the respective reactant, transition, and product states have all been optimized in an aqueous phase environment, and the vibrational frequencies are computed in the liquid phase assuming the timescale for reorientation of solvent molecules is much larger than the timescale for molecular vibrations. Implicit solvation calculations have been performed using both nonperiodic (iSMS)[41] and periodic (VASPsol)[69] approaches.

DOI: 10.1021/acs.jpcc.9b04994
J. Phys. Chem. C 2019, 123, 19052−19065

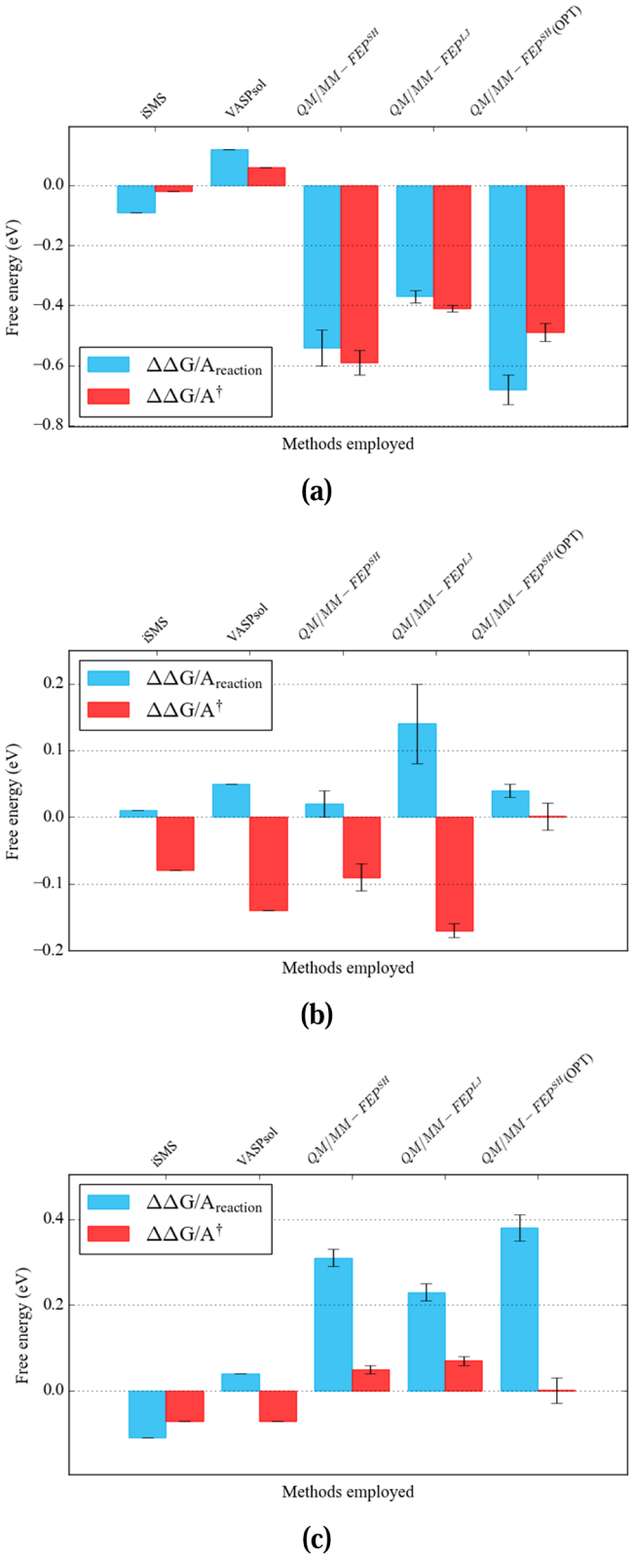

Figure 7. Effect of aqueous phase on the free energy of reaction and activation of (a) O−H, (b) C−H, and (c) C−OH bond cleavages of ethylene glycol over Pt(111) using different implicit and explicit solvation models. Error bars for the explicit solvation models are 95% confidence intervals.

use classical molecular mechanics simulations suffers from a fundamental issue, the accuracy and transferability of force fields.[103,133,134] To compare how the metal−water interaction potentials affect the reaction thermodynamics and kinetics, we have performed our QM/MM FEP calculations for the O−H, C−H, and C−OH bond cleavages of ethylene glycol with two different force-field parameters, the Spohr−Heinzinger (SH) potential[66] and Lennard-Jones (LJ) potential.[67] Figure S6 illustrates the distance distribution of water O atoms over a Pt(111) surface using the abovementioned metal−water interaction potentials. The LJ potential predicts a higher density of water molecules closer to the surface compared to the SH potential. Also, the highest water density is by ∼0.1 Å closer to the surface for the LJ potential, although some water molecules move slightly closer to the surface for the SH potential.

Table 1 and Figure 7 show the effect of these potentials on the thermodynamics and kinetics of our test reactions. The aqueous phase exerts an endergonic effect on the thermodynamics of the C−OH bond cleavage of ethylene glycol. While both the LJ and SH potentials predict only a nominal effect on the free energy of activation, the LJ potential predicts a less endergonic effect on the free energy of reaction (ΔA_{rxn}^{LJ} = 0.49 ± 0.02 eV) compared to that of the SH potential (ΔA_{rxn}^{SH} = 0.57 ± 0.02 eV). This phenomenon can likely be explained by the LJ potential having a higher water density closer to the surface (Figure S6), being able to at least somewhat stabilize the surface OH group in the product state (see Figure S7). Next, for the C−H bond cleavage, both Pt−water potentials predict similarly small solvation effects with the LJ potential predicting a minimally larger effect on the activation and reaction free energies. Finally, the LJ potential shows a less exergonic effect on the O−H bond scission of ethylene glycol compared to the SH potential. For the O−H cleavage of ethylene glycol, all stationary points are submerged in the surface water layer such that the effect of Pt−water potential originates likely from the difference in water density adjacent to the surface (Figure S6). While both potentials suggest that O−H bond dissociation is significantly accelerated and more exergonic in liquid water, intricacies of the potential lead to free-energy predictions deviating by as much as 0.2 eV. Given the large solvation effects for O−H bond dissociations, it appears that a more accurate/reliable Pt−water potential is required to predict solvation effects for the O−H bond cleavage with an accuracy comparable to DFT.

3.7. Comparison between Implicit and Explicit Solvation Methods. Finally, we compare our explicit solvation results to implicit solvation calculations performed with VASPsol[69,70] and our iSMS methodology.[41] Both implicit solvation models (iSMS and VASPsol) fail to capture the full solvent stabilization during the O−H cleavage of ethylene glycol (see Table 1 and Figure 7). However, VASPsol predicts even an endergonic effect on both the free energy of reaction and the free energy of activation for this model reaction. This prediction contradicts both of our predictions with iSMS and explicit solvation methodology (and are contradictory to our intuition and experimental studies).[128,135−140] For the C−H bond cleavage, implicit and explicit solvation models anticipate comparable solvent effects, which is plausible considering that directional hydrogen bonding contributions do not change significantly along the reaction coordinate for this reaction. Finally, for the C−OH bond cleavage, both implicit models do not predict the strong endergonic solvent effect on the reaction thermodynamics of the C−OH bond cleavage that results from the water molecules being unable to fully solvate the surface

DOI: 10.1021/acs.jpcc.9b04994
J. Phys. Chem. C 2019, 123, 19052−19065

OH group in the product state. To conclude, the reliability of implicit solvation calculations for heterogeneous (metal) catalysis applications is currently limited (unknown) due to the very limited availability of experimental data that can be used in the parameterization of the implicit solvation models. This is currently a clear advantage of explicit solvation models that rely "only" on a meaningful potential energy description.[121,132]

4. CONCLUSIONS

Very little experimental information is currently available to assess the accuracy of various computational approaches for predicting solvation effects on free energies of activation and free energies of reaction for elementary processes on heterogeneous catalysts. As a result, computational models can primarily only be compared against each other and chemical intuition. In principle, the most accurate computational solvation models use an explicit description of the solvent molecules and describe the potential energy surface at a high level of theory. This however requires sufficient configuration space sampling, which is usually not affordable for a high level of theory description of the potential energy surface. In this contribution, using the O−H splitting reaction of ethylene glycol over Pt(111) as a case study and characteristic reaction for various biomass platform molecule conversion reactions over noble metal catalysts, we studied the required timescale to reach thermal equilibrium, the sampling time scale necessary to explore the configuration space, and the size of the simulation system for obtaining reliable and converged free energies of activation and reaction with our eSMS methodology for studying solvation effects in heterogeneous catalysis. Due to the difficulty in determining the correlation time in free-energy calculations, we recommend that all explicit solvation calculations be repeated multiple times just as it is common for experiments. Only by repeating simulations at least three times can confidence intervals (resulting from insufficient configuration space sampling and intricacies from our QM/MM-FEP methodology) be estimated. Assuming our test reactions are characteristic for various reactions on metal surfaces, our heuristic recommendations lead to free energies with 95% confidence intervals of <0.1 eV.

After having established protocols for calculating solvent effects using multiscale models, we calculated solvent effects on the free energy of reaction and free energy of activation for primary dehydrogenation and dehydroxylation reactions of ethylene glycol at the hydroxyl group and α-C. Vapor-phase-optimized geometries were reoptimized in the aqueous phase environment, and vibrational contributions were calculated using numerical gradients and central differences with a 0.02 au step size, assuming nonequilibrium solvation. Our explicit solvation model predicts that aqueous phase effects are small (<0.1 eV) for the C−H bond cleavage and the activation barrier of the C−OH bond cleavage. In contrast, solvation effects are large (>0.35 eV) for the O−H bond cleavage and the reaction free energy of the C−OH bond scission. While the choice of a different Pt−water force field can lead to differences in predicted solvation effects of up to 0.2 eV, the differences are usually much smaller (<0.1 eV), and the trends are always the same. In contrast, implicit solvation models only qualitatively agree with the explicit solvation results for the C−H bond cleavage, and they are unable to anticipate the hydrogen bonding stabilization for the O−H and even the C−OH cleavage reactions.

■ ASSOCIATED CONTENT

Supporting Information

The Supporting Information is available free of charge on the ACS Publications website at DOI: 10.1021/acs.jpcc.9b04994.

Effect of equilibration time, sampling and system size on aqueous phase simulations, optimized structures in vapor and aqueous phases, time-dependent total energy and root-mean-square fluctuations of the potential energy, rotational correlation time estimation, oxygen height distribution function, and simulation snapshots (PDF)

■ AUTHOR INFORMATION

Corresponding Author

*E-mail: heyden@cec.sc.edu.

ORCID

Muhammad Faheem: 0000-0002-8336-6176

Andreas Heyden: 0000-0002-4939-7489

Notes

The authors declare no competing financial interest.

■ ACKNOWLEDGMENTS

Dr. Michael R. Shirts from the University of Colorado Boulder is gratefully acknowledged for help with the statistical analysis of our results and the implementation of the Bennett Acceptance Ratio (BAR) as the free-energy estimator. This research has been funded by the United States Department of Energy, Office of Basic Energy Sciences (DE-SC0007167). M.Z. acknowledges financial support from the National Science Foundation (OIA-1632824). Computing resources provided by the National Energy Research Scientific Computing Center (NERSC), Texas Advanced Computing Center (TACC), and Pacific Northwest National Laboratory (PNNL) are gratefully acknowledged.

■ REFERENCES

(1) In *Handbook of Solvents*, 2nd ed.; Wypych, G., Ed. ChemTec Publishing: Oxford, 2014; Vol. 2, pp 1−261.

(2) Claisen, L. Beiträge zur Kenntniss der 1,3 - Diketone und verwandter Verbindungen. *Justus Liebigs Ann. Chem.* **1896**, *291*, 25−137.

(3) Wislicenus, W. Ueber die Isomerie der Formylphenylessigester. *Justus Liebigs Ann. Chem.* **1896**, *291*, 147−216.

(4) Hantzsch, A. Zur Kenntniss der Säureamide. *Justus Liebigs Ann. Chem.* **1897**, *296*, 84−94.

(5) Reichardt, C.; Welton, T. In *Solvents and Solvent Effects in Organic Chemistry*, 4th, updated and enl. ed.; Reichardt, C., Welton, T., Eds.; Wiley-VCH: Weinheim, Germany, 2011.

(6) Menschutkin, N. Beiträge zur Kenntnis der Affinitätskoeffizienten der Alkylhaloide und der organischen Amine. *Z. Physik. Chem.* **1890**, *5U*, 589.

(7) Knowles, W. S. Asymmetric hydrogenation. *Acc. Chem. Res.* **2002**, *16*, 106−112.

(8) Valgimigli, L.; Banks, J. T.; Ingold, K. U.; Lusztyk, J. Kinetic Solvent Effects on Hydroxylic Hydrogen Atom Abstractions Are Independent of the Nature of the Abstracting Radical. Two Extreme Tests Using Vitamin E and Phenol. *J. Am. Chem. Soc.* **1995**, *117*, 9966−9971.

(9) Wiebus, E.; Cornils, B. Die großtechnische Oxosynthese mit immobilisiertem Katalysator. *Chem. Ing. Tech.* **1994**, *66*, 916−923.

DOI: 10.1021/acs.jpcc.9b04994
J. Phys. Chem. C 2019, 123, 19052−19065

(10) Beller, M.; Cornils, B.; Frohning, C. D.; Kohlpaintner, C. W. Progress in Hydroformylation and Carbonylation. *J. Mol. Catal. A: Chem.* **1995**, *104*, 17−85.
(11) Cornils, B. Exciting Results from the Field of Homogeneous Two-Phase Catalysis. *Angew. Chem., Int. Ed. Engl.* **1995**, *34*, 1575−1577.
(12) Cornils, B.; Wiebus, E. Aqueous Catalysts for Organic-Reactions. *Chemtech* **1995**, *25*, 33−38.
(13) Malleron, J. L.; Juin, A.; Nguyen, T. P. H.; Mhoumadi, C. *Database related to palladium-catalyzed organic chemistry*; International Union of Pure and Applied Chemistry: Washington, DC, 1995
(14) Phan, N. T.; Van Der Sluys, M.; Jones, C. W. On the nature of the active species in palladium catalyzed Mizoroki-Heck and Suzuki-Miyaura couplings - Homogeneous or heterogeneous catalysis, a critical review. *Adv. Synth. Catal.* **2006**, *348*, 609−679.
(15) Dyson, P. J.; Jessop, P. G. Solvent effects in catalysis: rational improvements of catalysts via manipulation of solvent interactions. *Catal. Sci. Technol.* **2016**, *6*, 3302−3316.
(16) Bini, R.; Chiappe, C.; Mestre, V. L.; Pomelli, C. S.; Welton, T. A rationalization of the solvent effect on the Diels-Alder reaction in ionic liquids using multiparameter linear solvation energy relationships. *Org. Biomol. Chem.* **2008**, *6*, 2522−2529.
(17) Breslow, R.; Guo, T. Diels-Alder reactions in nonaqueous polar solvents. Kinetic effects of chaotropic and antichaotropic agents and of .beta.-cyclodextrin. *J. Am. Chem. Soc.* **1988**, *110*, 5613−5617.
(18) Cornils, B.; Herrmann, W. A.; Eckl, R. W. Industrial aspects of aqueous catalysis. *J. Mol. Catal. A: Chem.* **1997**, *116*, 27−33.
(19) Rajadhyaksha, R. A.; Karwa, S. L. Solvent Effects in Catalytic-Hydrogenation. *Chem. Eng. Sci.* **1986**, *41*, 1765−1770.
(20) Mukherjee, S.; Vannice, M. A. Solvent effects in liquid-phase reactionsI. Activity and selectivity during citral hydrogenation on Pt/SiO2 and evaluation of mass transfer effects. *J. Catal.* **2006**, *243*, 108−130.
(21) Mukherjee, S.; Vannice, M. Solvent effects in liquid-phase reactions II. Kinetic modeling for citral hydrogenation. *J. Catal.* **2006**, *243*, 131−148.
(22) Akpa, B. S.; D'Agostino, C.; Gladden, L. F.; Hindle, K.; Manyar, H.; McGregor, J.; Li, R.; Neurock, M.; Sinha, N.; Stitt, E. H.; Weber, D.; Zeitler, J. A.; Rooney, D. W. Solvent effects in the hydrogenation of 2-butanone. *J. Catal.* **2012**, *289*, 30−41.
(23) McManus, I.; Daly, H.; Thompson, J. M.; Connor, E.; Hardacre, C.; Wilkinson, S. K.; Bonab, N. S.; Ten Dam, J.; Simmons, M. J. H.; Stitt, E. H.; D'Agostino, C.; McGregor, J.; Gladden, L. F.; Delgado, J. J. Effect of solvent on the hydrogenation of 4-phenyl-2-butanone over Pt based catalysts. *J. Catal.* **2015**, *330*, 344−353.
(24) Behtash, S.; Lu, J.; Walker, E.; Mamun, O.; Heyden, A. Solvent effects in the liquid phase hydrodeoxygenation of methyl propionate over a Pd(1 1 1) catalyst model. *J. Catal.* **2016**, *333*, 171−183.
(25) Behtash, S.; Lu, J.; Mamun, O.; Williams, C. T.; Monnier, J. R.; Heyden, A. Solvation Effects in the Hydrodeoxygenation of Propanoic Acid over a Model Pd(211) Catalyst. *J. Phys. Chem. C* **2016**, *120*, 2724−2736.
(26) Date, M.; Haruta, M. Moisture effect on CO oxidation over Au/TiO2 catalyst. *J. Catal.* **2001**, *201*, 221−224.
(27) Daté, M.; Okumura, M.; Tsubota, S.; Haruta, M. Vital role of moisture in the catalytic activity of supported gold nanoparticles. *Angew. Chem., Int. Ed.* **2004**, *43*, 2129−2132.
(28) Ebbesen, S. D.; Mojet, B. L.; Lefferts, L. In situ ATR-IR study of CO adsorption and oxidation over Pt/Al_2O_3 in gas and aqueous phase: Promotion effects by water and pH. *J. Catal.* **2007**, *246*, 66−73.
(29) Huang, J.; Akita, T.; Faye, J.; Fujitani, T.; Takei, T.; Haruta, M. Propene Epoxidation with Dioxygen Catalyzed by Gold Clusters. *Angew. Chem., Int. Ed.* **2009**, *48*, 7862−7866.
(30) Zope, B. N.; Hibbitts, D. D.; Neurock, M.; Davis, R. J. Reactivity of the Gold/Water Interface During Selective Oxidation Catalysis. *Science* **2010**, *330*, 74−78.
(31) Rossmeisl, J.; Skulason, E.; Björketun, M. E.; Tripkovic, V.; Norskov, J. K. Modeling the electrified solid-liquid interface. *Chem. Phys. Lett.* **2008**, *466*, 68−71.
(32) Miller, K. L.; Lee, C. W.; Falconer, J. L.; Medlin, J. W. Effect of water on formic acid photocatalytic decomposition on TiO2 and Pt/TiO2. *J. Catal.* **2010**, *275*, 294−299.
(33) Staszak-Jirkovsky, J.; Subbaraman, R.; Strmcnik, D.; Harrison, K. L.; Diesendruck, C. E.; Assary, R.; Frank, O.; Kobr, L.; Wiberg, G. K. H.; Genorio, B.; Connell, J. G.; Lopes, P. P.; Stamenkovic, V. R.; Curtiss, L.; Moore, J. S.; Zavadil, K. R.; Markovic, N. M. Water as a Promoter and Catalyst for Dioxygen Electrochemistry in Aqueous and Organic Media. *ACS Catal.* **2015**, *5*, 6600−6607.
(34) Cheng, T.; Xiao, H.; Goddard, W. A., III Free-Energy Barriers and Reaction Mechanisms for the Electrochemical Reduction of CO on the Cu(100) Surface, Including Multiple Layers of Explicit Solvent at pH 0. *J. Phys. Chem. Lett.* **2015**, *6*, 4767−4773.
(35) Zhang, L.; Karim, A. M.; Engelhard, M. H.; Wei, Z.; King, D. L.; Wang, Y. Correlation of Pt-Re surface properties with reaction pathways for the aqueous-phase reforming of glycerol. *J. Catal.* **2012**, *287*, 37−43.
(36) Tupy, S. A.; Karim, A. M.; Bagia, C.; Deng, W.; Huang, Y.; Vlachos, D. G.; Chen, J. G. Correlating Ethylene Glycol Reforming Activity with In Situ EXAFS Detection of Ni Segregation in Supported NiPt Bimetallic Catalysts. *ACS Catal.* **2012**, *2*, 2290−2296.
(37) Karim, A. M.; Howard, C.; Roberts, B.; Kovarik, L.; Zhang, L.; King, D. L.; Wang, Y. In Situ X-ray Absorption Fine Structure Studies on the Effect of pH on Pt Electronic Density during Aqueous Phase Reforming of Glycerol. *ACS Catal.* **2012**, *2*, 2387−2394.
(38) He, R.; Davda, R. R.; Dumesic, J. A. In situ ATR-IR spectroscopic and reaction kinetics studies of water-gas shift and methanol reforming on Pt/Al2O3Catalysts in vapor and liquid phases. *J. Phys. Chem. B* **2005**, *109*, 2810−2820.
(39) Taylor, C. D.; Neurock, M. Theoretical insights into the structure and reactivity of the aqueous/metal interface. *Curr. Opin. Solid State Mater. Sci.* **2005**, *9*, 49−65.
(40) Yoon, Y.; Rousseau, R.; Weber, R. S.; Mei, D.; Lercher, J. A. First-Principles Study of Phenol Hydrogenation on Pt and Ni Catalysts in Aqueous Phase. *J. Am. Chem. Soc.* **2014**, *136*, 10287−10298.
(41) Faheem, M.; Suthirakun, S.; Heyden, A. New Implicit Solvation Scheme for Solid Surfaces. *J. Phys. Chem. C* **2012**, *116*, 22458−22462.
(42) Cramer, C. J. *Essentials of Computational Chemistry: Theories and Models*; J. Wiley: West Sussex, England; New York, 2002; p xvii, p 542.
(43) Okamoto, Y. Density-functional calculations of atomic and molecular adsorptions on 55-atom metal clusters: Comparison with (111) surfaces. *Chem. Phys. Lett.* **2005**, *405*, 79−83.
(44) Okamoto, Y. Comparison of hydrogen atom adsorption on Pt clusters with that on Pt surfaces: A study from density-functional calculations. *Chem. Phys. Lett.* **2006**, *429*, 209−213.
(45) Car, R.; Parrinello, M. Unified Approach for Molecular-Dynamics and Density-Functional Theory. *Phys. Rev. Lett.* **1985**, *55*, 2471−2474.
(46) Carloni, P.; Rothlisberger, U.; Parrinello, M. The role and perspective of ab initio molecular dynamics in the study of biological systems. *Acc. Chem. Res.* **2002**, *35*, 455−464.
(47) Iftimie, R.; Minary, P.; Tuckerman, M. E. Ab initio molecular dynamics: Concepts, recent developments, and future trends. *Proc. Natl. Acad. Sci. U. S. A.* **2005**, *102*, 6654−6659.
(48) Hibbitts, D. D.; Neurock, M. Influence of oxygen and pH on the selective oxidation of ethanol on Pd catalysts. *J. Catal.* **2013**, *299*, 261−271.
(49) Chen, L. D.; Urushihara, M.; Chan, K.; Nørskov, J. K. Electric Field Effects in Electrochemical CO2Reduction. *ACS Catal.* **2016**, *6*, 7133−7139.
(50) Mattsson, T. R.; Paddison, S. J. Methanol at the water-platinum interface studied by ab initio molecular dynamics. *Surf. Sci.* **2003**, *544*, L697−L702.

DOI: 10.1021/acs.jpcc.9b04994
J. Phys. Chem. C 2019, 123, 19052−19065

(51) Otani, M.; Hamada, I.; Sugino, O.; Morikawa, Y.; Okamoto, Y.; Ikeshoji, T. Structure of the water/platinum interface - a first principles simulation under bias potential. *Phys. Chem. Chem. Phys.* **2008**, *10*, 3609−3612.
(52) Yang, J.; Dauenhauer, P. J.; Ramasubramaniam, A. The role of water in the adsorption of oxygenated aromatics on Pt and Pd. *J. Comput. Chem.* **2013**, *34*, 60−66.
(53) Klamt, A.; Schüürmann, G. J. G. J. COSMO: a New Approach to Dielectric Screening in Solvents with Explicit Expressions for the Screening Energy and Its Gradient. *J. Chem. Soc., Perkin Trans. 2* **1993**, 799−805.
(54) Saleheen, M.; Heyden, A. Liquid-Phase Modeling in Heterogeneous Catalysis. *ACS Catal.* **2018**, *8*, 2188−2194.
(55) Zhang, Y.; Liu, H.; Yang, W. Free energy calculation on enzyme reactions with an efficient iterative procedure to determine minimum energy paths on a combined ab initio QM/MM potential energy surface. *J. Chem. Phys.* **2000**, *112*, 3483−3492.
(56) Hu, H.; Lu, Z.; Yang, W. QM/MM minimum free-energy path: Methodology and application to triosephosphate isomerase. *J. Chem. Theory Comput.* **2007**, *3*, 390−406.
(57) Hu, H.; Lu, Z. Y.; Parks, J. M.; Burger, S. K.; Yang, W. Quantum mechanics/molecular mechanics minimum free-energy path for accurate reaction energetics in solution and enzymes: Sequential sampling and optimization on the potential of mean force surface. *J. Chem. Phys.* **2008**, *128*, No. 034105.
(58) Faheem, M.; Heyden, A. Hybrid Quantum Mechanics/Molecular Mechanics Solvation Scheme for Computing Free Energies of Reactions at Metal-Water Interfaces. *J. Chem. Theory Comput.* **2014**, *10*, 3354−3368.
(59) Salacuse, J. J.; Denton, A. R.; Egelstaff, P. A.; Tau, M.; Reatto, L. Finite-size effects in molecular dynamics simulations: Static structure factor and compressibility. II. Application to a model krypton fluid. *Phys. Rev. E* **1996**, *53*, 2390−2401.
(60) Castro-Roman, F.; Benz, R. W.; White, S. H.; Tobias, D. J. Investigation of finite system size effects in molecular dynamics simulations of lipid bilayers. *J. Phys. Chem. B* **2006**, *110*, 24157−24164.
(61) Lebowitz, J. L.; Percus, J. K. Long-Range Correlations in a Closed System with Applications to Nonuniform Fluids. *Phys. Rev.* **1961**, *122*, 1675−1691.
(62) Lebowitz, J. L.; Percus, J. K. Thermodynamic Properties of Small Systems. *Phys. Rev.* **1961**, *124*, 1673−1681.
(63) Mandell, M. J. On the properties of a Periodic Fluid. *J. Stat. Phys.* **1976**, *15*, 299−305.
(64) Pratt, L. R.; Haan, S. W. Effects of Periodic boundary conditions on Equilibrium Properties of computer simulated fluids. I. Theory. *J. Chem. Phys.* **1981**, *74*, 1864−1872.
(65) Faheem, M.; Saleheen, M.; Lu, J.; Heyden, A. Ethylene glycol reforming on Pt(111): first-principles microkinetic modeling in vapor and aqueous phases. *Catal. Sci. Technol.* **2016**, *6*, 8242−8256.
(66) Spohr, E. Computer-Simulation of the Water Platinum Interface. *J. Phys. Chem.* **1989**, *93*, 6171−6180.
(67) Heinz, H.; Vaia, R. A.; Farmer, B. L.; Naik, R. R. Accurate Simulation of Surfaces and Interfaces of Face-Centered Cubic Metals Using 12-6 and 9-6 Lennard-Jones Potentials. *J. Phys. Chem. C* **2008**, *112*, 17281−17290.
(68) Klamt, A. Conductor-Like Screening Model for Real Solvents - a New Approach to the Quantitative Calculation of Solvation Phenomena. *J. Phys. Chem.* **1995**, *99*, 2224−2235.
(69) Mathew, K.; Sundararaman, R.; Letchworth-Weaver, K.; Arias, T. A.; Hennig, R. G. Implicit solvation model for density-functional study of nanocrystal surfaces and reaction pathways. *J. Chem. Phys.* **2014**, *140*, No. 084106.
(70) Fishman, M.; Zhuang, H. L.; Mathew, K.; Dirschka, W.; Hennig, R. G. Accuracy of exchange-correlation functionals and effect of solvation on the surface energy of copper. *Phys. Rev. B* **2013**, *87*, 245402.
(71) Kresse, G.; Furthmüller, J. Efficiency of ab-initio total energy calculations for metals and semiconductors using a plane-wave basis set. *Comput. Mater. Sci.* **1996**, *6*, 15−50.
(72) Kresse, G.; Furthmüller, J. Efficient iterative schemes for ab initio total-energy calculations using a plane-wave basis set. *Phys. Rev. B* **1996**, *54*, 11169−11186.
(73) Blöchl, P. E. Projector Augmented-Wave Method. *Phys. Rev. B* **1994**, *50*, 17953−17979.
(74) Perdew, J. P.; Yue, W. Accurate and Simple Density Functional for the Electronic Exchange Energy - Generalized Gradient Approximation. *Phys. Rev. B* **1986**, *33*, 8800−8802.
(75) Perdew, J. P.; Wang, Y. Accurate and Simple Analytic Representation of the Electron-Gas Correlation-Energy. *Phys. Rev. B* **1992**, *45*, 13244−13249.
(76) Perdew, J. P.; Burke, K.; Ernzerhof, M. Generalized gradient approximation made simple. *Phys. Rev. Lett.* **1996**, *77*, 3865−3868.
(77) Monkhorst, H. J.; Pack, J. D. Special Points for Brillouin-Zone Integrations. *Phys. Rev. B* **1976**, *13*, 5188−5192.
(78) Methfessel, M.; Paxton, A. T. High-Precision Sampling for Brillouin-Zone Integration in Metals. *Phys. Rev. B* **1989**, *40*, 3616−3621.
(79) Makov, G.; Payne, M. C. Periodic boundary conditions in ab initio calculations. *Phys. Rev. B* **1995**, *51*, 4014−4022.
(80) Harris, J. Simplified Method for Calculating the Energy of Weakly Interacting Fragments. *Phys. Rev. B* **1985**, *31*, 1770−1779.
(81) Foulkes, W. M. C.; Haydock, R. Tight-Binding Models and Density-Functional Theory. *Phys. Rev. B* **1989**, *39*, 12520−12536.
(82) Henkelman, G.; Jónsson, H. Improved tangent estimate in the nudged elastic band method for finding minimum energy paths and saddle points. *J. Chem. Phys.* **2000**, *113*, 9978−9985.
(83) Henkelman, G.; Uberuaga, B. P.; Jónsson, H. A climbing image nudged elastic band method for finding saddle points and minimum energy paths. *J. Chem. Phys.* **2000**, *113*, 9901−9904.
(84) Henkelman, G.; Jónsson, H. A dimer method for finding saddle points on high dimensional potential surfaces using only first derivatives. *J. Chem. Phys.* **1999**, *111*, 7010−7022.
(85) Heyden, A.; Bell, A. T.; Keil, F. J. Efficient methods for finding transition states in chemical reactions: Comparison of improved dimer method and partitioned rational function optimization method. *J. Chem. Phys.* **2005**, *123*, 224101.
(86) Ahlrichs, R.; Bär, M.; Häser, M.; Horn, H.; Kölmel, C. Electronic-Structure Calculations on Workstation Computers - the Program System Turbomole. *Chem. Phys. Lett.* **1989**, *162*, 165−169.
(87) Treutler, O.; Ahlrichs, R. Efficient Molecular Numerical-Integration Schemes. *J. Chem. Phys.* **1995**, *102*, 346−354.
(88) Von Arnim, M.; Ahlrichs, R. Performance of parallel TURBOMOLE for density functional calculations. *J. Comput. Chem.* **1998**, *19*, 1746−1757.
(89) Schäfer, A.; Horn, H.; Ahlrichs, R. Fully Optimized Contracted Gaussian-Basis Sets for Atoms Li to Kr. *J. Chem. Phys.* **1992**, *97*, 2571−2577.
(90) Weigend, F.; Ahlrichs, R. Balanced basis sets of split valence, triple zeta valence and quadruple zeta valence quality for H to Rn: Design and assessment of accuracy. *Phys. Chem. Chem. Phys.* **2005**, *7*, 3297−3305.
(91) Russo, T. V.; Martin, R. L.; Hay, P. J. Effective Core Potentials for Dft Calculations. *J. Phys. Chem.* **1995**, *99*, 17085−17087.
(92) Eichkorn, K.; Weigend, F.; Treutler, O.; Ahlrichs, R. Auxiliary basis sets for main row atoms and transition metals and their use to approximate Coulomb potentials. *Theor. Chem. Acc.* **1997**, *97*, 119−124.
(93) Weigend, F. Accurate Coulomb-fitting basis sets for H to Rn. *Phys. Chem. Chem. Phys.* **2006**, *8*, 1057−1065.
(94) Todorov, I. T.; Smith, W.; Trachenko, K.; Dove, M. T. DL_POLY_3: new dimensions in molecular dynamics simulations via massive parallelism. *J. Mater. Chem.* **2006**, *16*, 1911−1918.
(95) Natarajan, S. K.; Behler, J. Neural network molecular dynamics simulations of solid-liquid interfaces: water at low-index copper surfaces. *Phys. Chem. Chem. Phys.* **2016**, *18*, 28704−28725.

DOI: 10.1021/acs.jpcc.9b04994
J. Phys. Chem. C 2019, 123, 19052−19065

(96) Jorgensen, W. L.; Chandrasekhar, J.; Madura, J. D.; Impey, R. W.; Klein, M. L. Comparison of Simple Potential Functions for Simulating Liquid Water. *J. Chem. Phys.* **1983**, *79*, 926−935.
(97) Andersen, H. C. Rattle - a Velocity Version of the Shake Algorithm for Molecular-Dynamics Calculations. *J. Comput. Phys.* **1983**, *52*, 24−34.
(98) Smith, W.; Forester, T. R. Parallel Macromolecular Simulations and the Replicated Data Strategy. *Comput. Phys. Commun.* **1994**, *79*, 63−77.
(99) Swope, W. C.; Andersen, H. C.; Berens, P. H.; Wilson, K. R. A Computer-Simulation Method for the Calculation of Equilibrium-Constants for the Formation of Physical Clusters of Molecules - Application to Small Water Clusters. *J. Chem. Phys.* **1982**, *76*, 637−649.
(100) Jorgensen, W. L. Optimized Intermolecular Potential Functions for Liquid Alcohols. *J. Phys. Chem.* **1986**, *90*, 1276−1284.
(101) Geerke, D. P.; Van Gunsteren, W. F. The performance of non-polarizable and polarizable force-field parameter sets for ethylene glycol in molecular dynamics simulations of the pure liquid and its aqueous mixtures. *Mol. Phys.* **2010**, *105*, 1861−1881.
(102) MacKerell, A. D., Jr.; Bashford, D.; Bellott, M. L. D. R.; Dunbrack, R. L., Jr.; Evanseck, J. D.; Field, M. J.; Fischer, S.; Gao, J.; Guo, H.; Ha, S.; Joseph-McCarthy, D.; Kuchnir, L.; Kuczera, K.; Lau, F. T. K.; Mattos, C.; Michnick, S.; Ngo, T.; Nguyen, D. T.; Prodhom, B.; Reiher, W. E.; Roux, B.; Schlenkrich, M.; Smith, J. C.; Stote, R.; Straub, J.; Watanabe, M.; Wiórkiewicz-Kuczera, J.; Yin, D.; Karplus, M. All-atom empirical potential for molecular modeling and dynamics studies of proteins. *J. Phys. Chem. B* **1998**, *102*, 3586−3616.
(103) Steinmann, S. N.; Ferreira De Morais, R.; Götz, A. W.; Fleurat-Lessard, P.; Iannuzzi, M.; Sautet, P.; Michel, C. Force Field for Water over Pt(111): Development, Assessment, and Comparison. *J. Chem. Theory Comput.* **2018**, *14*, 3238−3251.
(104) Reed, A. E.; Weinstock, R. B.; Weinhold, F. Natural-Population Analysis. *J. Chem. Phys.* **1985**, *83*, 735−746.
(105) Burow, A. M.; Sierka, M.; Döbler, J.; Sauer, J. Point defects in CaF_2 and CeO_2 investigated by the periodic electrostatic embedded cluster method. *J. Chem. Phys.* **2009**, *130*, 174710.
(106) Nosé, S. A Unified Formulation of the Constant Temperature Molecular-Dynamics Methods. *J. Chem. Phys.* **1984**, *81*, 511−519.
(107) Hoover, W. G. Canonical Dynamics - Equilibrium Phase-Space Distributions. *Phys. Rev. A* **1985**, *31*, 1695−1697.
(108) Essmann, U.; Perera, L.; Berkowitz, M. L.; Darden, T.; Lee, H.; Pedersen, L. G. A Smooth Particle Mesh Ewald Method. *J. Chem. Phys.* **1995**, *103*, 8577−8593.
(109) Cowan, M. L.; Bruner, B. D.; Huse, N.; Dwyer, J. R.; Chugh, B.; Nibbering, E. T. J.; Elsaesser, T.; Miller, R. J. D. Ultrafast memory loss and energy redistribution in the hydrogen bond network of liquid H2O. *Nature* **2005**, *434*, 199−202.
(110) Zwanzig, R. W. High-Temperature Equation of State by a Perturbation Method. I. Nonpolar Gases. *J. Chem. Phys.* **1954**, *22*, 1420−1426.
(111) Archontis, G.; Simonson, T.; Moras, D.; Karplus, M. Specific amino acid recognition by aspartyl-tRNA synthetase studied by free energy simulations. *J. Mol. Biol.* **1998**, *275*, 823−846.
(112) Zeng, J.; Fridman, M.; Maruta, H.; Treutlein, H. R.; Simonson, T. Protein-protein recognition: An experimental and computational study of the R89K mutation in Raf and its effect on Ras binding. *Protein Sci.* **1999**, *8*, 50−64.
(113) Best, S. A.; Merz, K. M., Jr; Reynolds, C. H. Free energy perturbation study of octanol/water partition coefficients: Comparison with continuum GB/SA calculations. *J. Phys. Chem. B* **1999**, *103*, 714−726.
(114) Shirts, M. R.; Pande, V. S. Comparison of efficiency and bias of free energies computed by exponential averaging, the Bennett acceptance ratio, and thermodynamic integration. *J. Chem. Phys.* **2005**, *122*, 144107.
(115) Lu, N.; Singh, J. K.; Kofke, D. A. Appropriate methods to combine forward and reverse free-energy perturbation averages. *J. Chem. Phys.* **2003**, *118*, 2977−2984.
(116) Ryde, U. How Many Conformations Need To Be Sampled To Obtain Converged QM/MM Energies? The Curse of Exponential Averaging. *J. Chem. Theory Comput.* **2017**, *13*, 5745−5752.
(117) Bennett, C. H. Efficient Estimation of Free Energy Differences from Monte Carlo Data. *J. Comput. Phys.* **1976**, *22*, 245−268.
(118) Shirts, M. R.; Bair, E.; Hooker, G.; Pande, V. S. Equilibrium free energies from nonequilibrium measurements using maximum-likelihood methods. *Phys. Rev. Lett.* **2003**, *91*, 140601.
(119) Kreyszig, E. *Advanced Engineering Mathematics*, 9th ed.; John Wiley & Sons: New York, 2006.
(120) Fernández, D. P.; Goodwin, A. R. H.; Lemmon, E. W.; Levelt Sengers, J. M. H.; Williams, R. C. A formulation for the static permittivity of water and steam at temperatures from 238 K to 873 K at pressures up to 1200 MPa, including derivatives and Debye−Hückel coefficients. *J. Phys. Chem. Ref. Data* **1997**, *26*, 1125−1166.
(121) Herron, J. A.; Morikawa, Y.; Mavrikakis, M. Ab initio molecular dynamics of solvation effects on reactivity at electrified interfaces. *Proc. Natl. Acad. Sci. U. S. A.* **2016**, *113*, E4937−E4945.
(122) Bulo, R. E.; Michel, C.; Fleurat-Lessard, P.; Sautet, P. Multiscale Modeling of Chemistry in Water: Are We There Yet? *J. Chem. Theory Comput.* **2013**, *9*, 5567−5577.
(123) Xie, T.; Sarupria, S.; Getman, R. B. A DFT and MD study of aqueous-phase dehydrogenation of glycerol on Pt(1 1 1): comparing chemical accuracy versus computational expense in different methods for calculating aqueous-phase system energies. *Mol. Simul.* **2017**, *43*, 370−378.
(124) Zhang, X.; DeFever, R. S.; Sarupria, S.; Getman, R. B. Free Energies of Catalytic Species Adsorbed to Pt(111) Surfaces under Liquid Solvent Calculated Using Classical and Quantum Approaches. *J. Chem. Inf. Model.* **2019**, *59*, 2190.
(125) Walker, E.; Ammal, S. C.; Terejanu, G. A.; Heyden, A. Uncertainty Quantification Framework Applied to the Water-Gas Shift Reaction over Pt-Based Catalysts. *J. Phys. Chem. C* **2016**, *120*, 10328−10339.
(126) Hu, H.; Yang, W. Development and application of ab initio QM/MM methods for mechanistic simulation of reactions in solution and in enzymes. *J. Mol. Struct.: THEOCHEM* **2009**, *898*, 17−30.
(127) de Souza, O. N.; Ornstein, R. L. Effect of periodic box size on aqueous molecular dynamics simulation of a DNA dodecamer with particle-mesh Ewald method. *Biophys. J.* **1997**, *72*, 2395−2397.
(128) Zhang, X.; Sewell, T. E.; Glatz, B.; Sarupria, S.; Getman, R. B. On the water structure at hydrophobic interfaces and the roles of water on transition-metal catalyzed reactions: A short review. *Catal. Today* **2017**, *285*, 57−64.
(129) Michel, C.; Zaffran, J.; Ruppert, A. M.; Matras-Michalska, J.; Jędrzejczyk, M.; Grams, J.; Sautet, P. Role of water in metal catalyst performance for ketone hydrogenation: a joint experimental and theoretical study on levulinic acid conversion into gamma-valerolactone. *Chem. Commun.* **2014**, *50*, 12450−12453.
(130) Desai, S. K.; Pallassana, V.; Neurock, M. A periodic density functional theory analysis of the effect of water molecules on deprotonation of acetic acid over Pd(111). *J. Phys. Chem. B* **2001**, *105*, 9171−9182.
(131) Liu, Y.; Gregersen, B. A.; Hengge, A.; York, D. M. Transesterification thio effects of phosphate diesters: Free energy barriers and kinetic and equilibrium isotope effects from density-functional theory. *Biochemistry* **2006**, *45*, 10043−10053.
(132) Schweitzer, B.; Steinmann, S. N.; Michel, C. Can micro-solvation effects be estimated from vacuum computations? A case-study of alcohol decomposition at the H2O/Pt(111) interface. *Phys. Chem. Chem. Phys.* **2019**, *21*, 5368.
(133) Behler, J.; Parrinello, M. Generalized neural-network representation of high-dimensional potential-energy surfaces. *Phys. Rev. Lett.* **2007**, *98*, 146401.
(134) Behler, J. Representing potential energy surfaces by high-dimensional neural network potentials. *J. Phys.: Condens. Matter* **2014**, *26*, 183001.

DOI: 10.1021/acs.jpcc.9b04994
J. Phys. Chem. C 2019, 123, 19052−19065

(135) Desai, S. K.; Neurock, M. First-principles study of the role of solvent in the dissociation of water over a Pt-Ru alloy. *Phys. Rev. B* **2003**, *68*, No. 075420.
(136) Hibbitts, D. D.; Loveless, B. T.; Neurock, M.; Iglesia, E. Mechanistic Role of Water on the Rate and Selectivity of Fischer-Tropsch Synthesis on Ruthenium Catalysts. *Angew. Chem., Int. Ed.* **2013**, *52*, 12273−12278.
(137) Santana, J. A.; Mateo, J. J.; Ishikawa, Y. Electrochemical Hydrogen Oxidation on Pt(110): A Combined Direct Molecular Dynamics/Density Functional Theory Study. *J. Phys. Chem. C* **2010**, *114*, 4995−5002.
(138) Skachkov, D.; Venkateswara Rao, C.; Ishikawa, Y. Combined First-Principles Molecular Dynamics/Density Functional Theory Study of Ammonia Electrooxidation on Pt(100) Electrode. *J. Phys. Chem. C* **2013**, *117*, 25451−25466.
(139) Nie, X.; Luo, W.; Janik, M. J.; Asthagiri, A. Reaction mechanisms of CO_2 electrochemical reduction on Cu(111) determined with density functional theory. *J. Catal.* **2014**, *312*, 108−122.
(140) Huang, Z. Q.; Long, B.; Chang, C. R. A theoretical study on the catalytic role of water in methanol steam reforming on PdZn(111). *Catal. Sci. Technol.* **2015**, *5*, 2935−2944.

DOI: 10.1021/acs.jpcc.9b04994
J. Phys. Chem. C 2019, 123, 19052−19065